焊接残余应力对 2024 铝合金薄板疲劳寿命的影响

张正伟，　张　昭，　张洪武
（大连理工大学 工业装备结构分析国家重点实验室，大连　116024）

摘　要： 对搅拌磨擦焊、TIG 焊和激光焊进行数值模拟，得到焊接残余应力场. 将残余应力场施加到线弹性断裂力学模型之中，运用 J 积分方法计算残余应力强度因子，并计算裂纹扩展速率，通过与试验结果和虚拟裂纹闭合法计算结果进行对比，验证了文中所使用方法的正确性. 研究发现，残余应力强度因子的分布与残余应力分布形式相似. 残余应力的引入，对应力比有较大影响，但随着应力比的增大，残余应力对应力比的影响逐渐减弱. 焊接残余应力的引入缩短了焊接构件的使用寿命，当裂纹长度较小时，TIG 焊接构件使用寿命比搅拌摩擦焊接构件和激光焊接构件使用寿命短.

关键词： 焊接残余应力场；J 积分；残余应力强度因子；裂纹扩展速率
中图分类号： TG 405　　**文献标识码：** A　　**文章编号：** 0253－360X(2014)10－0029－04

0　序　　言

焊接技术已经被广泛应用于航空航天、船舶与汽车等工业领域[1]. 与传统的铆接技术相比，焊接技术的使用减少了产品的制造成本，降低了产品重量，具有明显优势[2]. 但焊接结构经受循环载荷时，残余应力会影响其损伤容限和构件的使用寿命. Bussu 等人[3]研究指出裂纹扩展速率依赖于裂纹方向和裂纹相对于焊缝的位置. Servetti 等人[4]研究了焊接残余应力对裂纹扩展速率的影响，将试验残余应力场引入有限元模型，基于计算残余应力强度因子并预测裂纹扩展速率.

尽管已有针对残余应力对裂纹扩展速率及焊接结构服役寿命影响的研究工作，但比较不同焊接工艺所产生残余应力场对裂纹扩展速率及结构服役寿命的影响还鲜见报道. 文中通过数值方法研究了搅拌摩擦焊(FSW)、TIG 焊和激光焊(LW)残余应力场对裂纹扩展速率及构件使用寿命的影响.

1　模型描述

1.1　顺序热力耦合模型

焊接薄板尺寸均为 200 mm×40 mm×4 mm，采用八节点六面体线性单元进行网格划分，如图 1 所示焊缝区域网格尺寸为 0.5 mm×0.5 mm×0.5 mm. TIG 焊和激光焊，热源尺寸较小且焊接热流密度较大，焊缝区域采用 0.5 mm×0.25 mm×0.25 mm 网格，可以更好的捕捉热源信息. 材料为 2024 铝合金，密度为 2 770 kg/m^3，泊松比为 0.33，比热容为 875 J/(kg·℃)，热应力计算采用 Johnson-Cook 材料模型.

图 1　薄板有限元模型
Fig. 1　Finite element model for welding plate

采用移动热源模拟焊接过程中热输入量，搅拌摩擦焊(FSW)热源可表示为[5-7]

$$q_s(x,y,z) = \frac{3Q_s\sqrt{(x-x_0-vt)^2+y^2}}{2\pi(R_2^3-R_1^3)} \quad (1)$$

$$q_p = \frac{Q_p}{\pi R_1^2 H} \quad (2)$$

式中：Q_s 和 Q_p 表示搅拌头的轴肩和搅拌针所产生的热输入功率；R_2 为搅拌头的轴肩半径，为 9.5 mm；R_1 和 H 为搅拌针半径和高度，分别为 3.125 mm 和 4 mm；x_0 表示焊接起始位置；v 为焊接速度；q_s 为面热源热流密度；q_p 为体热源热流密度.

TIG 焊与激光焊都采用高斯热源进行模拟，可

收稿日期：2013－04－12
基金项目：国家自然科学基金资助项目(10802017)；国家重点基础研究发展计划资助项目(973 计划，2010CB832704)；国家高技术研究发展计划资助项目(863 计划，2012AA050901)；新世纪优秀人才支持计划资助项目(NCET-12-0075)；中央高校基本科研业务费专项资金资助项目

表示为[8,9]

$$q_r = \frac{3Q}{\pi R_0^2}\exp\left(-\frac{3(x^2+y^2)}{R_0^2}\right) \quad (3)$$

式中: Q 为热输入功率,对于 TIG 焊,$Q = hUI$,h 为焊接效率,为 0.38; U 和 I 为电弧电压和焊接电流,分别为 180 V 和 12 A. 对于激光焊接,$Q = h_L P_0$,h_L 和 P_0 分别为激光吸收率和激光焊接输入功率,其中激光吸收率取 0.68,激光焊接输入功率为 1 000 W,R_0 为热源有效半径.

1.2 断裂力学模型

文中研究残余应力对含有中间裂纹薄板使用寿命的影响,基于线弹性断裂力学建立了二维断裂力学模型. 裂纹尖端第一层单元采用蜕化单元,可以模拟裂纹尖端应力奇异,外层为八节点四边形单元,作为 J 积分计算区域. 应力变化范围为 45 MPa,应力比为 0.1 ~0.8 时,计算外载荷作用下最大应力强度因子 $K_{app,max}$ 和最小应力强度因子 $K_{app,min}$. 通过 Abaqus 子程序 SIGINI 施加焊接残余应力场,计算残余应力强度因子 K_{res}.

采用 NASGRO 方程预测裂纹扩展速率,即

$$\frac{da}{dN} = C\left[\left(\frac{1-f}{1-R}\right)\Delta K_{app}\right]^n \frac{\left(1-\frac{\Delta K_{th}}{\Delta K_{app}}\right)^p}{\left(1-\frac{K_{app,max}+K_{res}}{K_{crit}}\right)^q} \quad (4)$$

式中: C,n 为材料常数; R 为应力比; ΔK_{app} 为应力强度因子变化范围; ΔK_{th} 与 K_{crit} 分别为应力强度因子门槛值和临界应力强度因子; p 和 q 为形状系数; f 为裂纹闭合率. 由式(4)可知,裂纹扩展速率为裂纹长度 a 的函数,可表示为 $g(a)$,则式(4)可表示为

$$dN = \frac{da}{g(a)} \quad (5)$$

对式(5)进行积分即可求得构件使用寿命.

2 方法验证

选取 Liljedahl 等人[2]和 Servetti 等人[4]工作进行方法验证. J 积分方法计算残余应力强度因子与虚拟裂纹闭合法(virtual crack closure technique,VCCT)[4]方法计算残余应力强度因子对比如图 2 所示. 结果吻合良好. NASGRO 方程预测裂纹扩展速率与试验[2]结果对比如图 3 所示,结果吻合良好,验证了文中所使用方法的正确性.

3 结果讨论

搅拌摩擦焊、TIG 焊和激光焊残余应力场如图 4 所示,最大值分别为 116,180 和 217 MPa. TIG 焊和激光焊最大残余应力远大于搅拌摩擦焊残余应力. 在远离焊缝区域,焊接残余应力都表现为压应力,且搅拌摩擦焊接残余压应力大于其它两种焊接形式.

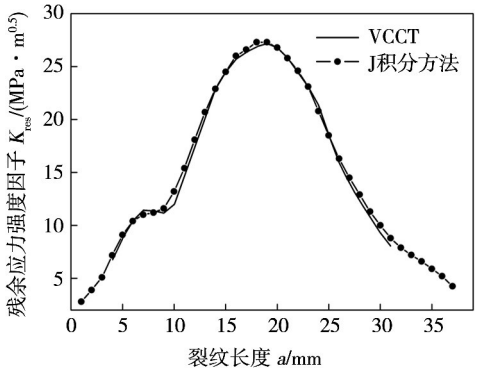

图 2 预测结果与 VCCT 方法对比

Fig. 2 Comparison of prediction and VCCT result

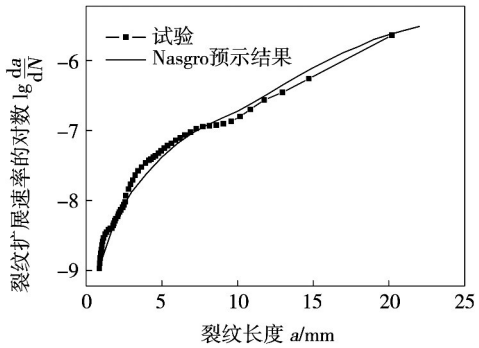

图 3 预测结果与试验结果对比

Fig. 3 Comparison of prediction and experiment

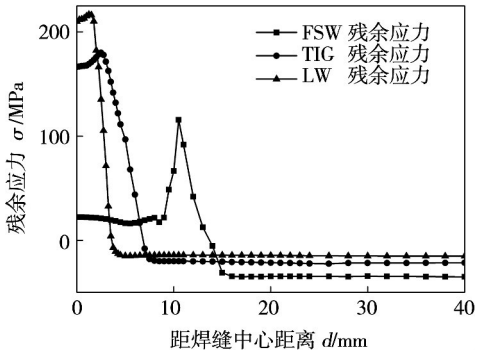

图 4 搅拌摩擦焊和 TIG 焊及激光焊纵向残余应力场分布

Fig. 4 Residual stress distribution of FSW, TIG and LW

搅拌摩擦焊残余应力强度因子从焊缝中心位置到轴肩外侧位置逐渐增大,远离轴肩的位置残余应力强度因子逐渐减小(图 5). TIG 焊接和激光焊接残余应力强度因子最大值都出现在焊缝边缘位置.

残余应力对应力比的影响如图6所示. 对于

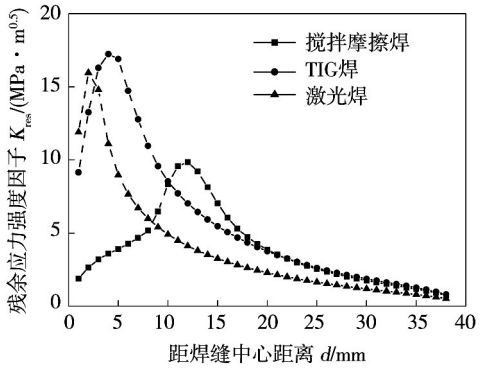

图 5　残余应力强度因子分布情况

Fig. 5　Distribution residual stress intensity factor

TIG 焊和激光焊，焊缝位置残余应力对应力比的影响最大，应力比分别增加了 170% 和 180%，远离焊缝位置残余应力的影响逐渐减小. 对于搅拌摩擦焊，R_{eff}的最大值出现在搅拌头的轴肩外侧位置，R_{eff}为 0.604，增大了 101%.

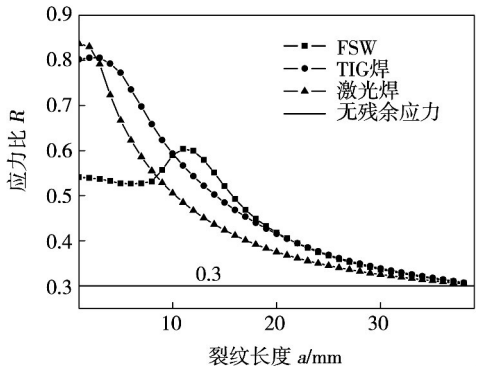

图 6　残余应力对 R 的影响

Fig. 6　Influence of the residual stress on R

R 分别取 0.3，0.5 和 0.8 时，搅拌摩擦焊接产生的残余应力对 R 的影响如图 7 所示. 当 R 为 0.3 时，残余应力对其的影响最大. 但随着 R 的增大，残余应力对其影响逐渐减弱. 当 R 为 0.8 时，R_{eff}最大值为 0.836，只增大了 4.5%. 可知应力变化范围不变时，应力比越大，残余应力对应力比的影响越小.

使用搅拌摩擦焊、TIG 焊和激光焊，其有效应力比和裂纹扩展速率如图 8 所示. 靠近焊缝中线区域，TIG 焊和激光焊薄板裂纹扩展速率大于搅拌摩擦焊接薄板裂纹扩展速率，且裂纹长度 $a > 3$ mm 时，TIG 焊薄板裂纹扩展速率大于激光焊薄板裂纹扩展速率. 当裂纹长度在 11 ~ 20 mm 之间时，搅拌摩擦焊薄板裂纹扩展速率大于其余两种焊接薄板裂纹扩展速率. 对比残余应力强度因子和裂纹扩展速率曲线可知，当 K_{res}相同时，采用不同焊接形式的薄

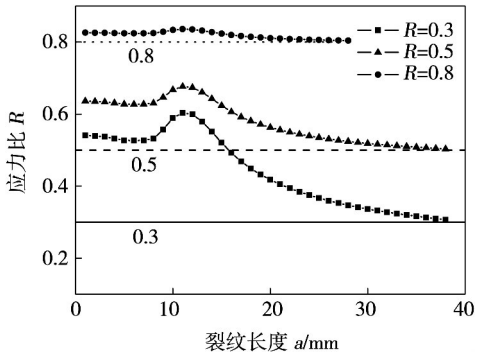

图 7　搅拌摩擦焊接残余应力对 R 的影响

Fig. 7　Influence of residual stresses of friction stir welding on R

板具有相同的裂纹扩展速率. 因此，可以通过对比不同残余应力场下残余应力强度因子，研究不同残余应力场对裂纹扩展速度的影响.

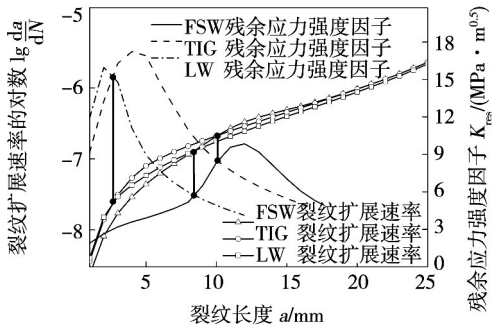

图 8　裂纹扩展速率与残余应力强度因子(R = 0.3)

Fig. 8　Fatigue crake growth rate and K_{res}(R = 0.3)

不同焊接形式残余应力对裂纹扩展速率的影响如图 9 和图 10 所示. 随着 R 的增大，残余应力对裂纹扩展速率的影响逐渐减弱. 同种焊接形式下，裂纹尺寸相同时，裂纹扩展速率随着 R 的增大而增大.

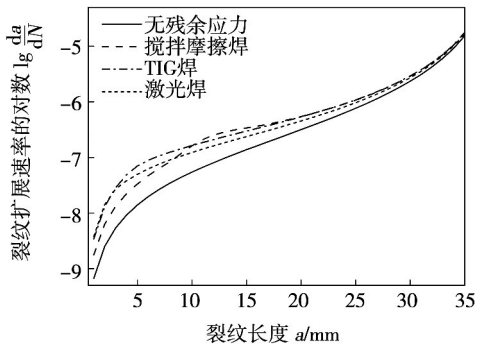

图 9　R = 0.1 不同焊接形式残余应力对裂纹扩展速率的影响

Fig. 9　Influence of weld patterns on FCGR at R = 0.1

为了研究焊接残余应力对构件使用寿命的影响，对裂纹扩展速率进行积分，计算构件使用寿命.

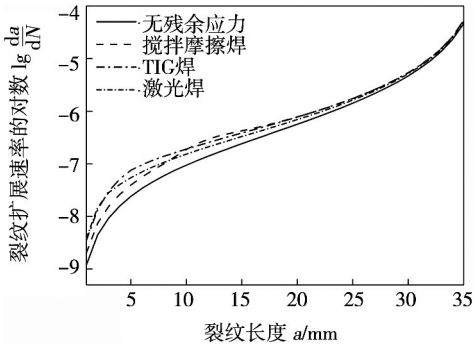

图 10 $R=0.3$ 不同焊接形式残余应力对裂纹扩展速率的影响

Fig. 10 Influence of weld patterns on FCGR at $R=0.3$

裂纹尺寸为 1 mm 应力比为 0.3 时，构件使用寿命曲线如图 11 所示. 无残余应力时，需要进行 849 979 次循环，构件才能破坏. 经过搅拌摩擦焊、TIG 焊与激光焊的构件分别需要 506 293 次、300 328 次和 316 325 次循环，构件完全断裂. 因此，焊接残余应力的引入，显著的降低了构件的使用寿命. 3 种焊接技术分别使构件寿命降低了 40.4%，64.7% 和 62.8%.

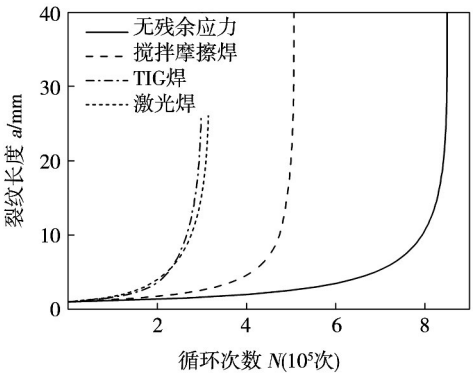

图 11 $R=0.3$，$a=1$ mm 构件使用寿命预测

Fig. 11 Prediction of fatigue life at $R=0.3$，$a=1$ mm

裂纹尺寸为 5 mm 应力比为 0.3 时，构件使用寿命曲线如图 12 所示.

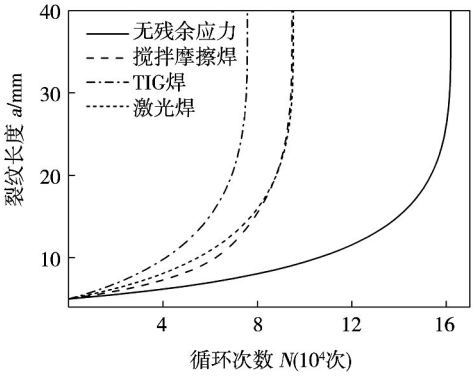

图 12 $R=0.3$，$a=5$ mm 构件使用寿命预测

Fig. 12 Prediction of fatigue life at $R=0.3$，$a=5$ mm

无残余应力时，构件破坏循环次数为 161 944，搅拌摩擦焊、TIG 焊与激光焊残余应力分别使构件寿命缩短了 41.2%，53.2% 和 41.2%.

4 结 论

(1) 激光焊接构件的最大残余应力大于 TIG 焊和搅拌摩擦焊接构件，而搅拌摩擦焊接残余应力仅为 116 MPa，远小于材料屈服极限.

(2) 焊接残余应力影响有效应力比的分布形式，但随着应力比的增大，其影响逐渐减弱.

(3) 对于相同尺寸薄板，可以通过比较残余应力强度因子来判断不同残余应力场对裂纹扩展速率的影响.

(4) 随着应力比的增大，裂纹扩展速率逐渐增大，而残余应力对裂纹扩展速率的影响逐渐减弱.

(5) 焊接残余应力缩短了构件的使用寿命，裂纹为 1 mm 时，搅拌摩擦焊接构件使用寿命大于其余两种焊接构件. 裂纹长度为 5 mm 时，搅拌摩擦焊接和激光焊接构件几乎具有相同的使用寿命，且大于 TIG 焊接构件的使用寿命.

参考文献:

[1] 张 华，林三宝，吴 林，等. 搅拌摩擦焊研究进展及前景展望[J]. 焊接学报. 2003，24(3)：91－96.
Zhang Hua，Lin Sanbao，Wu Lin，*et al*. Current progress and prospect of friction stir welding [J]. Transactions of the China Welding Institution，2003，24(4)：91－96.

[2] Liljedahl C D M，Tan M L，Zanellato O，*et al*. Evolution of residual stresses with fatigue loading and subsequent crack growth in a welded aluminium alloy middle tension specimen [J]. Engineering Fracture Mechanics，2008，75：3881－3894.

[3] Bussu G，Irving P E. The role of residual stress and heat affected zone properties on fatigue crack propagation in friction stir welded 2024-T351 aluminium joints [J]. International Journal of Fatigue，2003，25：77－88.

[4] Servetti G，Zhang X. Predicting fatigue crack growth rate in a welded butt joint：the role of effective R ratio in accounting for residual stress effect [J]. Engineering Fracture Mechanics，2009，76：1589－1602.

[5] 张正伟，张 昭，张洪武. 搅拌摩擦焊接残余应力及残余变形数值分析[J]. 计算力学学报. 2013，30(s)：16－21.
Zhang Zhengwei，Zhang Zhao，Zhang Hongwu. Investigations on residual stress and residual distortion of friction stir welding [J]. Chinese Journal of Computational Mechanics. 2013，30(s)：16－21.

[6] 张正伟，张 昭，刘亚丽，等. 搅拌摩擦焊数值模拟过程中不同转速与热输入功率之间关系研究[J]. 焊接. 2012(4)：19－24.

[下转第 36 页]

(2) 在温度200 ℃,压力10 MPa,保温30 min的烧结条件下,利用覆纳米银铜粉和纳米银颗混合焊膏烧结的焊接界面结合紧密,在焊接接头组织中可观察到纳米银与覆纳米银铜粉相互扩散,并且存在一定的孔隙率. 与之对比的纳米银焊膏单独低温烧结时,焊接界面结合紧密无空隙,只在界面处银铜相互扩散形成薄层固溶体,接头内组织有也有一定的孔隙率,但低于上述混合焊膏.

参考文献:

[1] 邹贵生,闫剑锋,母凤文,等. 微连接和纳连接的研究新进展[J]. 焊接学报,2011,32(4):107-112.
Zou Guisheng, Yan Jianfeng, Mu Fengwen, *et al*. Recent progress in micro-joining and nano-joining [J]. Transactions of the China Welding Institution, 2011, 32(4): 107-112.

[2] 马 良,尹力梦,冼健威,等. 高温电子封装无铅化的研究进展[J]. 焊接技术,2009,38(5):6-10.
Ma Liang, Yin Limeng, Xian Jianwei, *et al*. Research advancement of high temperature lead-free electronic packaging [J]. Welding Technology, 2009, 38(5): 6-10.

[3] Herring C. Effect of change of scale on sintering phenomena [J]. Journal of Applied Physics, 1950, 21: 301-303.

[4] Morisada Y, Nagaoka T, Fukusumi M, *et al*. A low-temperature bonding process using mixed Cu-Ag nanoparticles [J]. Journal of Electronic Materials, 2010, 39(8): 283-288.

[5] Kim S, Siow R. Mechanical properties of nano-silver joints as die-attach materials [J]. Journal of Alloys and Compounds, 2012, 514: 6-19.

[6] Morisada Y, Nagaoka T, Fukusumi M, *et al*. A low-temperature-bonding process usingmixed Cu-Ag nano-particles [J]. Journal of-Electronic Materials, 2010, 39(8): 283-288.

[7] Yan J F, Zou G S, Mu F W, *et al*. A study onlow temperature sintering-bonding of Cu metal bulks with Ag-nan-oparticle powders for high temperature electronics [C] // The proceedings of 2nd Advanced Welding & Joining Technology Conference and International Forum on Recent Advances in Welding Science and Technology. Harbin, China, 2011: 138-145.

[8] Choi S Y, Kang S. Sintering kinetics by structural transition at grain boundaries in barium titanate [J]. Acta Materialia, 2004, 52(10): 2937-2943.

作者简介: 曹 洋,女,1991年出生,硕士研究生. 主要从事新材料及其异种材料连接方面的研究工作. Email: caoyang_yly@163.com

通讯作者: 何 鹏,男,教授,博士研究生导师. Email: hithepeng@hit.edu.cn

[上接第32页]

Zhang Zhengwei, Zhang Zhao, Liu Yalin, *et al*. Investigation on relationship between the rotational speed and the input power in the simulation of FSW [J]. Welding & Joining, 2012(4): 19-24.

[7] Zhang Z W, Zhang Z, Zhang H W. Numerical investigations of size effects on residual states of friction stir weld [J]. Proceedings of the Institution of Mechanical Engineers, Part B: Journal of Engineering Manufacture, 2014, 228: 572-581.

[8] 薛忠明,顾 兰,张彦华. 激光焊接温度场数值模拟[J]. 焊接学报,2003,24(2):79-82.
Xue Zhongming, Gu Lan, Zhang Yanhua. Numerical simulation on temperature field in laser welding [J]. Transactions of the China Welding Institution, 2003, 24(2): 79-82.

[9] 马 琳,原津萍,张 平,等. 多道激光熔覆温度场的有限元数值模拟[J]. 焊接学报,2007,28(7):109-112.
Ma Lin, Yuan Jinping, Zhang Ping, *et al*. Finite numerical simulation of temperature field in multi-pass laser cladding [J]. Transactions of the China Welding Institution, 2007, 28(7): 109-112.

作者简介: 张正伟,男,1985年出生,博士研究生. 主要从事焊接构件疲劳性能和残余状态研究. 发表论文5篇. Email: zzw216@mail.dlut.edu.cn

通讯作者: 张洪武,男,博士,教授,博士研究生导师. Email: zhanghw@dlut.edu.cn

tandem submerged arc welding of grade X80 pipeline steel is developed by using finite element analysis software ANSYS. The element birth-death technique is employed to deal with the filling of double-V groove along the longitudinal seam of pipeline steel, and double-ellipsoid volumetric heat source is used to achieve the thermo-load application and solution. The calculated results show that the phenomenon, three-wire in a single weld pool, emerges at 1.6 s after the weld starting, the quasi-steady state is achieved at 6 s, and then a weld pool with length of over 100 mm is produced. The three peak values of temperature at the thermal cycles in weld and heat affected zone elongate the high temperature dwelling time of the thermal cycles, which is the main reason why the grains in the heat affected zone become coarser and the joint properties worsen. The comparison between the experimental and predicted results shows that the agreement extent of the weld width is better than that of the weld penetration, and the calculation accuracy can be improved if the weld reinforcement is considered.

Key words: pipeline steel; multi-wire tandem submerged arc welding; heat affected zone; thermal cycle; numerical simulation

Research on rapid underwater welding based on SHS

YIN Yujun, PAN Chuanzeng, SU Shan (Department of Vehicle and Electric Engineering, Mechanical Engineering College, Shijiazhuang 050003, China). pp 21 – 24

Abstract: Based on SHS technology, rapid underwater welding was investigated. The solder was composed of thermite of $CuO + Cu_2O + Al$, gasification agent of $CaCO_3$, alloy agent of $FeSi + MnFe$ and slagging agents of B_2O_3. The weld block was consisted of graphite crucible and rectangular pipe, meanwhile, one end of rectangular pipe was sealed and another one sealed partly to control the heating direction of combustion flame. Tungsten coil was used to ignite KNO_3/Al-Mg ignition materials and the paraffin was used to seal the opening of the weld block. Finally, the feasibility problem of underwater welding based on SHS was solved. It was found that, this technology can be operated easily without power supply to form welded joints after self-combustion of the solder in weld block. Welded joints with tensile strength of 135 MPa can be obtained under the condition of water depth of 0.5 m, and the emergency repairs of underwater damaged structures can be realized basically.

Key words: underwater welding; self-propagation; emergency repairs; welding mechanism

Microstructure and mechanical properties of variable polarity plasma arc keyhole weld of 2A12 aluminum alloy

JIANG Yi[1,2], LIU Ming[2], LU Yaohui[2], XU Binshi[2] (1. Logistics academy, Naval University of Engineering, Tianjin 300450, China; 2. National Key Laboratory for Remanufacturing, Academy of Armored Forces Engineering, Beijing 100072, China). pp 25 – 28

Abstract: Variable polarity plasma arc welding, an efficient and cost-efficient welding technology, has been widely applied to aircraft components manufacture, especially aluminum alloy components. Variable polarity plasma arc keyhole weld of 2A12 aluminum alloy was conducted by welding torch with assistant nozzles under high welding speed and high heat input, and microstructure and mechanical properties of weld zone was analyzed as well. Due to the compression of assistant nozzles to plasma arc, crown weld is narrowed, however, root weld is broadened; reinforcements of both welds are increased. In the weld, fine equiaxed nondendritic grains are dominate, strengthening phases are with Al_2Cu phases largely and few S phases. Mechanical properties of weld zone are determined by the size and quantity of Al_2Cu. It could be concluded that the difference of hardness between parent metal and weld is little. Furthermore, microhardness distribution curve alongside longitudinal direction of weld is like U-shape, plain in the middle of weld and fluctuating in both sides of the crown and root weld.

Key words: variable polarity plasma arc; aluminum alloy; keyhole weld; mechanical properties

Influence of welding residual stresses on fatigue life of Al 2024 plate

ZHANG Zhengwei, ZHANG Zhao, ZHANG Hongwu (State Key Laboratory of Structural Analysis for Industrial Equipments, Dalian University of Technology, Dalian 116024, China). pp 29 – 32, 36

Abstract: Sequential coupled thermo-mechanical model and fracture mechanical model based on finite element method and J-integral method are established to calculate the residual stress and the stress intensity factor for friction stir welding, TIG and laser welding process, respectively. The commerical code NASGRO is used to predict the fatigue crack growth rate. This method is validated by comparing with the experimental data and results of the virtual crack closure technique method. The distribution of the residual stress intensity factor is similar with the residual stress profile and the residual stress has a significant impact on the effective stress ratio R. The influence decreases as the increase of the stress ratio. The residual stresses severely shorten the fatigue life of the plate, and the fatigue life of the plate welded with TIG technology is shorter than the ones of the plates welded with friction stir welding and laser welding.

Key words: welding residual stresses; J-intergral; residual stress intensity factor; fatigue crack growth rate

Preparation and connectivity of sintering paste containing copper particles covered by nano-silver

CAO Yang[1,2], LIU Ping[1], WEI Hongmei[2], LIN Tiesong[2], HE Peng[2], GU Xiaolong[1] (1. Zhejiang Province Key Laboratory of Soldering & Brazing Materials and Technology, Zhejiang Metallurgical Research Institute Co. Ltd., Hangzhou 310030, China; 2. State Key Laboratory of Advanced Welding and Joining, Harbin Institute of Technology, Harbin 150001, China). pp 33 – 36

Abstract: A kind of sintering paste mixed of nano-silver and copper particles covered by nano-silver was made, by which oxygen-free copper pad with 99.99% purity were connected at low temperature. Firstly, nano-silver particles whose average diameter were 20 – 35 nm were synthesized by liquid chemical reduction method. Meanwhile the copper particles covered by nano-silver were prepared by the method of chemical plating. Afterwards, these two kinds of particles were mixed by mechanical method to prepare sintering paste, by which oxygen free copper plate with 99.99% purity were joined under the condition of 10 MPa, 200 ℃ for 30 min. Finally, the microstructure of sintering section was observed by the scanning electron microscope (SEM). The results showed that the connection interface was sintered compactly, and certain porosities existed throughout the joint organization. The everge shear strength of the joints was about 20 MPa.

Key words: nano-silver; copper particles covered by nano-silver; low temperature connection